Probabilistic Meteorological Characterization for Turbine Loads

M Kelly[1], **G Larsen, N K Dimitrov, and A Natarajan**
Department of Wind Energy,
Risø Campus, Technical University of Denmark, Roskilde 4000, DK

E-mail: mkel@dtu.dk

Abstract. Beyond the existing, limited IEC prescription to describe fatigue loads on wind turbines, we look towards probabilistic characterization of the loads via analogous characterization of the atmospheric flow, particularly for today's "taller" turbines with rotors well above the atmospheric surface layer. Based on both data from multiple sites as well as theoretical bases from boundary-layer meteorology and atmospheric turbulence, we offer probabilistic descriptions of shear and turbulence intensity, elucidating the connection of each to the other as well as to atmospheric stability and terrain. These are used as input to loads calculation, and with a statistical loads output description, they allow for improved design and loads calculations.

1. Introduction

Given the increase in sizes and hub heights of horizontal-axis wind turbines over the last decades, typical wind turbine rotors can frequently be located mostly or entirely above the atmospheric surface layer (ASL), or even rising above the top of the atmospheric boundary layer (ABL); ABL depths range from ~150–1500m, with ASL depth being ~10% of the ABL depth. Due to this, with the yet more complex physics and numerous additional phenomena that occur above the already complicated ASL, it becomes sensible to adopt a probabilistic approach for describing the atmosphere as 'felt' by wind turbines. Further, the current IEC standard 61400-1 [1] does not yet treat the variability of shear, nor the subsequent implication upon turbulence intensity for wind turbine loads calculations, in a systematic manner. Thus we pursue statistical characterization of the atmospheric boundary layer for use in wind load calculations, in order to provide a more complete functional description for wind engineers, and ultimately for turbine design.

2. Atmospheric characterization; theory, statistics, and representation

Towards a statistical description of relevant atmospheric variables for load calculations, we focus on wind speed, its vertical derivative (shear), and turbulence intensity. To be useful, such description should not be merely empirically based; as such we attempt to relate to extant formulations and with basis in atmospheric boundary layer theory.

[1] To whom any correspondence should be addressed.

2.1. Data used for analysis

For this work we use data from a collection of sites, which all meet certain criteria: they must have multiple measurement heights, of which at least one should be significantly above 100m, with data recorded over an integer number of years. The criteria address the range of heights that correspond to turbine rotors, *above* the ASL; the statistics also need to be as representative as possible in a long-term sense, without e.g. seasonal biases. The sites considered are Cabauw in the Netherlands [2], Høvsøre [3] and Østerild [4] in Denmark, and a (confidential) commercial site (hereafter labeled 'MR') in the northeast US; Table 1 summarizes the sites used.

Table 1. Sites used, with upper, mid-rotor, and lower heights for shear exponent analysis; wind direction ranges; terrain types; and instrumentation.

Site	z_{upper} (m)	z_{mid} (m)	z_{lower} (m)	Dir. range	terrain type	Obs. type	Series length (y)
Cabauw	200	140	80	120–240°	farmland	Sonic	2
Høvsøre	160	100	60	60–120°	farmland	Sonic	6
Østerild	200/140	140/80	80/45	all	forest-mixed	Lidar	1
'MR'	136	80	40	all	mixed-forest	cup	1

The sites used vary in character, but they are all located in essentially flat terrain. The Østerild site has lidar data, so we do not use it for turbulence calculations. Due to the availability at many heights via lidar, it has been split into two sets, one "low" and one "high", to highlight differences between the statistics at different heights. The Østerild site is located in forest, with treetops less than 20m above ground, and the lowest lidar observation level (45m) is chosen to be above the subsequent roughness sub-layer [5] and above the effects of tree-induced flow-distortion for valid lidar use [6]; the terrain beyond several kilometers upwind also includes mixed grassland/agricultural and scattered forest. The site MR has similar characteristics, including forest with clearings for several km surrounding the mast, and mixed forest and farm/grassland farther away; both Østerild and 'MR' sites have winds prevailing from the west, though data were not filtered for direction. For both Høvsøre and Cabauw, relatively homogeneous wind sectors were chosen, dominated by farm and grassland; the length of data records (4 and 6 years respectively) allowed such directional filtering. Again the total number of sites was limited to 4, due to the difficulty of finding 'tall' measurements which meet the criteria (and also have high data-recovery rates and without problems e.g. flow distortion).

2.2. Shear exponent, distributions and application

Turbines are *indirectly* affected by atmospheric stability, terrain influences, and a number of atmospheric mechanisms, via the *effects* of these on the flow—as seen primarily through the wind shear and turbulence intensity which directly affect turbine loads. Thus we begin with the shear exponent α, defined implicitly by the IEC standard 61400-1 [1] and often in wind engineering [7–9] through the power-law relation for wind speed U at height z relative to wind speed at hub height z_{hub}: $U(z) = U(z_{hub})\left(z/z_{hub}\right)^{\alpha}$. This can be inverted to give a more direct and useful definition of shear exponent,

$$\alpha \equiv \frac{dU\,/\,dz}{U\,/\,z}. \tag{1}$$

This is a 'centered' definition where U and shear (dU/dz) are both evaluated at z, which facilitates use of α in derivations and subsequent relation to other quantities, as shown later. It is compatible with the form $\alpha = \ln[U(z_2)/U(z_1)]/\ln(z_2/z_1)$ used commonly since Irwin [7]; we use this form in our calculations and find little difference from (1). The wind speed is typically taken in wind energy applications as a 10-minute average, and in this paper we will be looking at statistics built upon

collections of 'data points' each comprised of such an average, including wind speed and variance of streamwise turbulent fluctuations.[2]

An indicator of the character of a potential turbine site is the distribution, i.e. probability density function $P(\alpha)$, of shear exponent. This is shown in figure 1a for all wind speeds above 3m/s at the sites we consider, again with Østerild broken into 'low' and 'high' cases. From the figure we see that the Høvsøre case has a peak at α a bit lower than the other sites, but otherwise the distributions overlap significantly and do not appear markedly different.

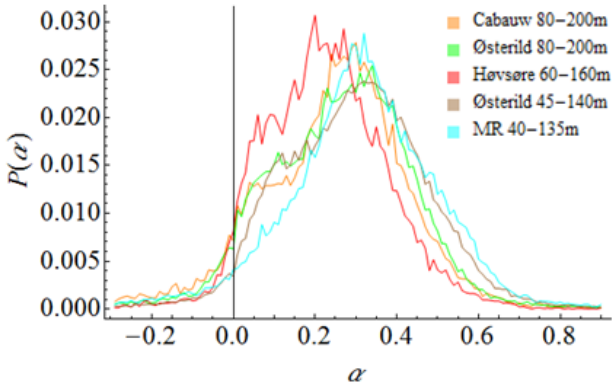

Figure 1. Shear exponent distributions for cases considered, all wind speeds above 3m/s.

One expects a wind-speed dependence in the probability of finding a given shear exponent, i.e. the joint-distribution $P(\alpha,U)$ is not trivial. Indeed this is the case, as shown in figure 2 for the sites considered. The figure shows a general narrowing of $P(\alpha|U)$ around lower α as U increases, with the effect more pronounced at the more homogeneous (non-forested) sites (given the similar z-ranges used); this is consistent with there being less effect of stability for high winds, and more turbulent transport affecting the shear over forest (discussed later). Also, one begins to see more differences between the sites, with the peak of $P(\alpha,U)$ occurring at lower U for lower z.[3]

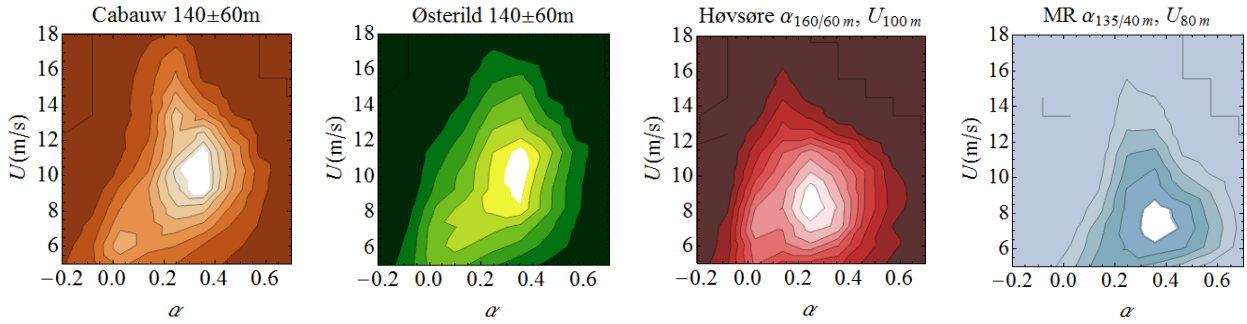

Figure 2. Joint distributions of wind speed $U(z_{mid})$ and shear exponent α, for Cabauw (orange, z_{mid}=140m), Østerild (green, z_{mid}=140m), Høvsøre (red, z_{mid}=100m), and commercial site 'MR' (blue, z_{mid}=80m). Heights used per site are listed in Table 1.

[2] We remind the reader that averages of second (and higher) order moments, such as turbulence fluctuations, require longer averaging times to ensure the same amount of random 'sampling' error as a first moment such as mean wind speed [21]; e.g. 30-minutes is more effective when considering turbulence than 10-minutes, but this aspect is outside the scope of the present paper.

[3] More generally, for lower z/z_0.This happens despite the peaks of the wind distribution (not shown) occurring in a different order (but with similar magnitude) due to different large-scale forcing or wind climate at the various locations. This insensitivity to site-dependent forcing is an attractive feature of α, arising from its 'normalized' dimensionless aspect.

2.2.1. Effective roughness above the ASL. Because near-neutral conditions tend to be encountered most often [10], the distribution of shear exponent can in neutral conditions be related to an effective roughness length. This may be seen when considering that for a logarithmic profile, (1) gives $\alpha_0 = 1/\ln(z/z_0)$. The concept is further demonstrated by figure 3a, which shows the distribution $P(\alpha)$ for both neutral and all conditions in the Høvsøre case. The peak of $P(\alpha)$ for the whole distribution is roughly the same as the peak of the distribution under neutral conditions, which happens in this case to coincide with the IEC [1] recommendation of 0.2; this corresponds to an effective roughness length $z_{0\text{eff}}$ exceeding 60 cm, which is much larger than the known surface roughness of several cm. If we consider the joint distribution of shear exponent and turbulence intensity in neutral conditions for this case, as shown in figure 3b, then we find a peak α_0 of ~1/6, corresponding to $z_{0\text{eff}}$ ~25cm, still larger than z_0. We can also look at the joint distribution of wind speed and α, comparable to figure 2, but in neutral conditions, as shown in figure 3c. The $P(\alpha,U)$ plot implies a peak α_0~1/7, particularly for increasing U; this matches the wind engineering rule-of-thumb [8] but corresponds to a roughness of ~9cm, also higher than measured for the site. All three effective roughnesses are larger than the conventional surface roughness of 1-3cm determined via log-law in the ASL, but this is not unexpected: for heights increasing above the ASL, the 'footprint' of (vertical) momentum fluxes becomes larger, with a larger upstream area affecting the observed winds; the effective roughness is increased as more variations in surface roughness [11] and/or terrain elevation [12] are encountered over a larger area [13]. Thus the roughness $z_{0\text{eff}}$ 'sensed' by the wind profile over a rotor well above the ASL will depend upon the classic surface roughness z_0,[4] but will be augmented beyond that based on inhomogeneity in upstream z_0 and the height above ground, relative to the variability in terrain elevation (i.e. the local scale or magnitude of elevation features in the vertical).[5]

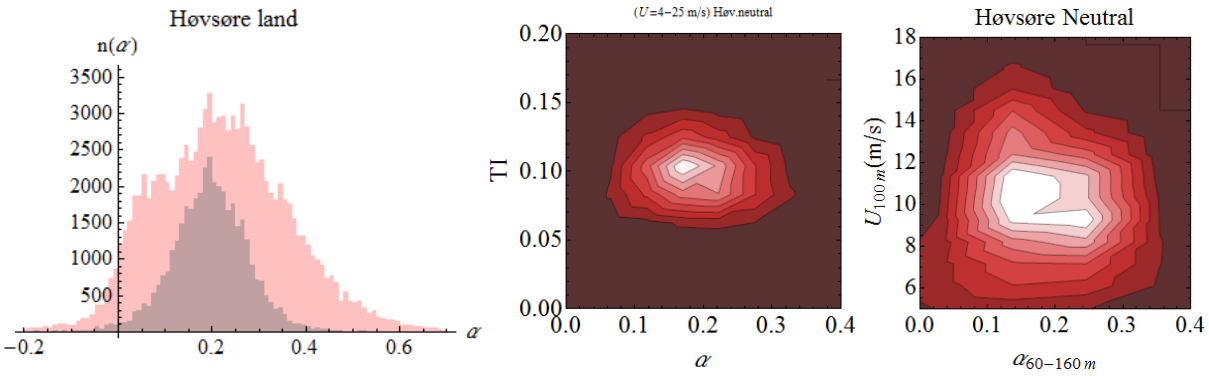

Figure 3. Left (a): histogram of shear exponent from Høvsøre, for both neutral (gray), and all conditions (pink). Center (b): joint distribution $P(\alpha,I_u)$ of α and turbulence intensity for near-neutral conditions. Right (c): joint distribution $P(\alpha,U)$ for neutral conditions.

As seen in figure 3c, one also witnesses an increase in shear due to the effect of increased winds above the top of the ABL as well as related jets (tending to occur most for easterly winds at Høvsøre when $U_{100\text{m}}$~9m/s), but we do not consider this as part of the effective roughness. Further, there is generally an increase in the mean shear exponent for lower wind speeds at the sites considered, consistent with the increased drag seen by e.g. [14] for weaker winds.

[4] We note that fits to $U(z/z_0)$ in the neutral surface layer (not shown here) also give a distribution of roughness lengths, analogous to the $P(\alpha)$ shown here. The average of such dictates the accepted surface roughness length, but unfortunately the character of the distribution and subsequent averaging is rarely documented.
[5] Mahrt [13] also summarizes the possible influence of the scale of heterogeneities upon the effective roughness.

As a function of wind speed, the mean shear exponent $\langle \alpha | U \rangle$ (or inverse $z_{0\text{eff}}$) will tend to increase from cut-in speed (~3–5m/s) to a somewhat constant value for a range of moderate wind speeds, and then potentially decline, shown in figure 4. However, if one filters out data corresponding to the lower half of turbulence intensities observed (not shown), then $\langle \alpha | U \rangle$ reaches a constant value without declining (similar to the green line in figure 4 for the high Østerild case), consistent with [15]. Just as with the peaks in $P(\alpha, U)$, the high-wind value of $\langle \alpha | U \rangle$ for the largest half of turbulence intensities (or the peak in all conditions as in figure 4) tends to increase with the effective surface roughness. In the interest of site-independent turbine load characterization, this $z_{0,\text{eff}}$-dependence can itself be gauged via turbulence intensity—higher roughnesses and terrain variations lead to stronger turbulence.

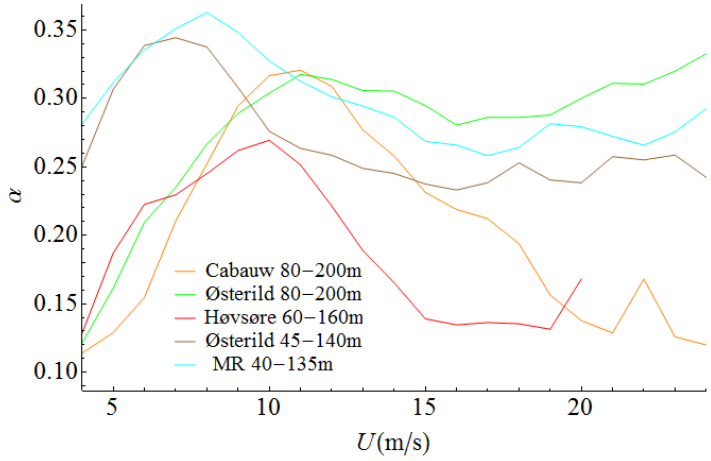

Figure 4. Mean shear exponent as a function of wind speed, $\langle \alpha | U \rangle$.

2.2.2. Stability and shear distributions. Turbines are not directly affected by heat fluxes or thermal stratification, but rather by atmospheric stability's effect on the flow, and so in wind engineering the stability is not considered, but its effect on shear, turbulence intensity, and mean wind speed are acknowledged. Here we probe the connection between distributions of stability and shear exponent. Following classical Monin-Obukhov theory [16], stability can be cast in terms of (inverse) Obukhov length $L^{-1} = (\kappa g / \theta_0)\overline{w\theta} / (\overline{uw})^{3/2}$ based on near-surface fluxes of heat $\left(\overline{w\theta}\right)$ and momentum $\left(\overline{uw} \equiv -u_*^2\right)$, where κ=0.4 is the von Kármán constant, g=9.8ms^{-2} is acceleration due to gravity, and θ_0 is the ASL mean potential temperature in K (overbars indicate 10-minute averages of fluctuating quantities).

The distribution of stability, $P(L^{-1})$, tends to have a peak near $L^{-1} = 0$ for sites on land, corresponding to zero heat flux from the surface. [10] found it could be described by a two-sided form $P(L^{-1}) \propto \exp\left(-|L^{-1}|^{2/3}\right)$. In the ASL where the wind speed profile can be represented by Monin-Obukhov theory, then (1) becomes $\alpha = \phi(z/L) / \left(\ln(z/z_0) - \psi(z/L)\right)$; this can be exploited under stable conditions (where $\psi_+(z/L) \simeq -5z/L$ and $\phi_+(z/L) \simeq 1 + 5z/L$) along with a probability transformation from $P(\alpha)$ to $P(L^{-1})$, to find a corresponding $P_+(\alpha_+)$ for the stable regimes that result in most instances of large shear exponents (see Appendix for details). Doing so, we obtain an analytical shear exponent distribution, which is shown in Figure 5 for the case of Høvsøre using measured ASL heat and momentum fluxes. While the stability distribution can be mapped somewhat reasonably in the ASL to a corresponding α distribution, the mapping fails for the Høvsøre case considered above the ASL (from 60–160m); further, replacing z_0 in the mapping with (larger) effective roughnesses (as found from e.g. figure 3) only degrades the results compared to the observed $P_+(\alpha_+)$.

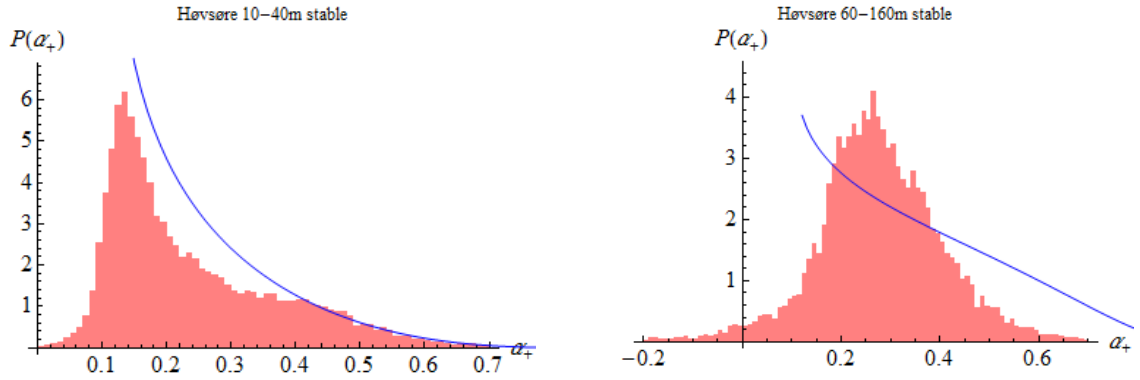

Figure 5. Shear exponent distribution $P_+(\alpha_+)$ predicted via stability distribution $P(L^{-1})$ for stable conditions (blue line) and measured distribution (red), Høvsøre case. Left: for ASL, z=10-40m; right: z=60-160m.

While one may analytically connect the distribution of stability to the shear distribution $P(\alpha)$ as we have just shown, above the ASL this does not produce reasonable results, because there is not necessarily a unique or 1:1 mapping between the two distributions. This is due in part to the wind at 160m sometimes being decoupled from the stable ASL flow, and more generally is caused by the turbulent kinetic energy balance being more complicated than assumed by Monin-Obukhov theory (i.e. in the ASL over flat terrain). The failure of the mapping is also consistent with the difficulties found by [9] in their attempt to relate turbulence intensity to stability, as will be seen below.

2.2.3. Variability of shear exponent. The distribution of shear exponent has a characteristic width, connected to the expected variability of α. Since the joint-distribution $P(\alpha,U)$ has a 2-dimensional shape (as in figure 2), then we expect that the shear variability will have a wind-speed dependence. The variance of α is $\sigma_\alpha^2(U) = \int \alpha^2 P(\alpha,U) d\alpha$ for a given (range of) U, but we lack an analytical form for $P(\alpha,U)$. However, we can get a hint about $\sigma_\alpha(U)$ by looking at the differential of (1), which can be written as $\delta\alpha = U^{-1}\left[z\,\delta(dU/dz) - \alpha\,\delta U\right]$: a combination of a 'turbulence' or shear piece (variation in dU/dz) and a 'Weibull' or mean wind piece (δU), together divided by U. Thus one might expect

$$\sigma_\alpha \propto U^{-1}. \tag{3}$$

One may also infer a dependence such as (3) by considering the turbulent kinetic energy budget, as in the next section. Indeed for the sites analyzed, we find that (3) applies in a basic sense, shown in Figure 6. As seen in the figure the standard deviation of shear exponent, calculated over 1 m/s bins of wind speed for the sites considered, tends to collapse around $1/U$. This is consistent also with the $P(\alpha,U)$ contours tending to come to a 'point' at higher U in Figure 2.

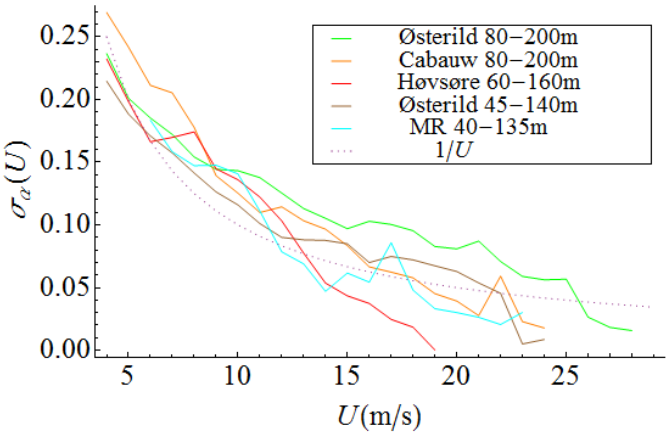

Figure 6. Standard deviation of shear exponent, for sites considered. Dotted line is U^{-1}.

The case with most inhomogeneous conditions and largest generalized roughness (Østerild high-z case) also have higher σ_α; conversely the case with both the most homogeneous upwind surface and smallest roughness (Høvsøre) has relatively smaller variation in α for wind speeds above 15 m/s—though the latter is also due in part to a lack of high-wind data from the homogeneous land sector at Høvsøre.

2.3. Turbulence intensity and shear exponent

When shear production of turbulent kinetic energy is not completely dominant, i.e. when a logarithmic profile or similarity theory may not apply, then relating shear and turbulence statistics becomes more complicated. To examine the relationship of these, one may consider the budget of turbulent kinetic energy, *e*. For steady (on average) conditions it can be written in simplified form as

$$\frac{de}{dt} = 0 = -\overline{uw}\frac{dU}{dz} + B + T - \varepsilon \tag{4}$$

where $\overline{uw}$ is the turbulent flux of streamwise momentum, ε is the dissipation, $B = (g/\theta_0)\overline{w\theta}$ is buoyant production or destruction, and T is turbulent kinetic energy transport. Then using (1), in general we have

$$\alpha = \frac{z}{U}\frac{(\varepsilon - B - T)}{-\overline{uw}} \tag{5}$$

at a given height *z*. In the (ASL) limit that all fluxes are constant with height, using $-\overline{uw} = u_{*0}^2$ and taking $\varepsilon = u_{*0}^3/\kappa z$ [17], then dividing (5) by (*U*/*z*) and using (1) we obtain

$$\alpha \simeq \frac{u_{*0}}{\kappa U} - \frac{gz\overline{w\theta}}{\theta_0 u_{*0}^2 U} - \frac{T}{u_{*0}^2 U / z}. \tag{5}$$

If one takes $\sigma_U \approx 2.5u_*$ (e.g. [1,8]) and uses the definition of Obukhov length, for vanishing transport then the shear exponent can be written more clearly in terms of turbulence intensity $I_U = \sigma_U / U$, and in line with Monin-Obukhov theory:

$$\alpha \simeq I_U\left[1 + \frac{z}{L}\right]. \tag{6}$$

Thus we have the sensible result that α increases conditions become more stable, and also with height in the ASL. We can see in the surface-layer neutral limit (i.e. a balance between shear production and viscous dissipation) the shear exponent becomes roughly equal to the turbulence intensity.

Above the ASL, in the regime of focus in this paper, however, (6) is of limited validity. One way to address this is via local similarity, which introduces a dependence upon boundary-layer depth h into the fluxes in (5) and (6). Using local similarity (e.g. [18]) gives a form like (5) for α, generally following $\alpha = \left(u_{*0}/\kappa U\right)\left[(1-z/h)^{a} + (z/L)(1-z/h)^{-b}\right]$ where h is the ABL depth and (a,b) are constants of order 1, and can be extended to include transport; however this has not yet been validated and is the subject of ongoing work.

As in the previous section, the behavior of the 'amplitude' of variations in α can be gleaned by considering its differential. Previously (1) was used, now (6) gives again a turbulence contribution and mean wind piece, both with a $1/U$ dependence, but now there is also a stability component: $\delta\alpha \sim U^{-1}(1+z/L)[\delta\sigma_U - I_U \delta U] + z\delta L^{-1}$. We note that the actual dependence will be more complicated than this above the ASL, with a yet more height-dependent result including ABL depth.

2.3.1. Simplified relations between α and I_U for standards. There is a need to relate the distributions of α and I_U, or at least the most likely of each, for the purpose of standardized loads calculations. Thus a relation such as (6) needs to be replaced by one where the stability is implicit within the turbulence intensity and shear exponent, with a form that is expressed in terms of reference values—compatible with the IEC 61400-1 standard.

A simple way to achieve such a relation is by extending Monin-Obukhov profile theory (see e.g. [10]), within α and I_U. Using $dU/dz = u_{*0}\phi(z/L)/(\kappa z)$ and $U = u_*[\alpha_0^{-1} - \psi(z/L)]/\kappa$, if we use a simplified form $\psi = \beta z/L$ [6], then we can write both α and I_U in terms of z/L. Eliminating $\beta z/L$ via α gives $I_U =_0 \kappa(\sigma_U/u_{*0})\alpha_0(1-\alpha)/(1-\alpha_0)$. If we take $\sigma_U \approx a_u u_*$ (where a_u is a constant typically taken to be 2.5, c.f.[1]), then defining the neutral, reference turbulence intensity as $I_{U0} \equiv a_u \kappa \alpha_0$, we have

$$I_U = \frac{I_{U0}}{1 + (\alpha - \alpha_0)/(1-\alpha)} \tag{7}$$

regardless of the choice of either β or a_u. The factor $(\alpha-\alpha_0)/(1-\alpha)$ arose from the stability term $\beta z/L$; realizing that (7) should be simplified for use above the ASL, and that the $(1-\alpha)$ part becomes more of a constant as other terms (such as transport) affect the shear there, we parameterize this factor as $c_\alpha(\alpha-\alpha_0)$ to get the engineering form

$$I_U = \frac{I_{U0}}{1 + c_\alpha(\alpha - \alpha_0)} \tag{8}$$

where the constant c_α is empirically found to be roughly 4.

Because the IEC 61400-1 uses a reference turbulence intensity at 15m/s, and because there is less variation of I_U at such speeds, we choose I_{U0} to correspond to such a reference, as well as analogously assigning α_0 (at 15m/s) for the same reasons. Doing so, we obtain the results shown in figure 7, using the simplified form (8). The figure shows $P(\alpha, I_U)$ for the sites having turbulence measurements, with the form (8) superposed as a line on top.

[6] β is a constant between 0 and 5, and the form reflects the larger impact of stable conditions on $U(z)$ relative to unstable conditions [10]; $\phi = 1 - z\,\mathrm{d}\psi/dz$.

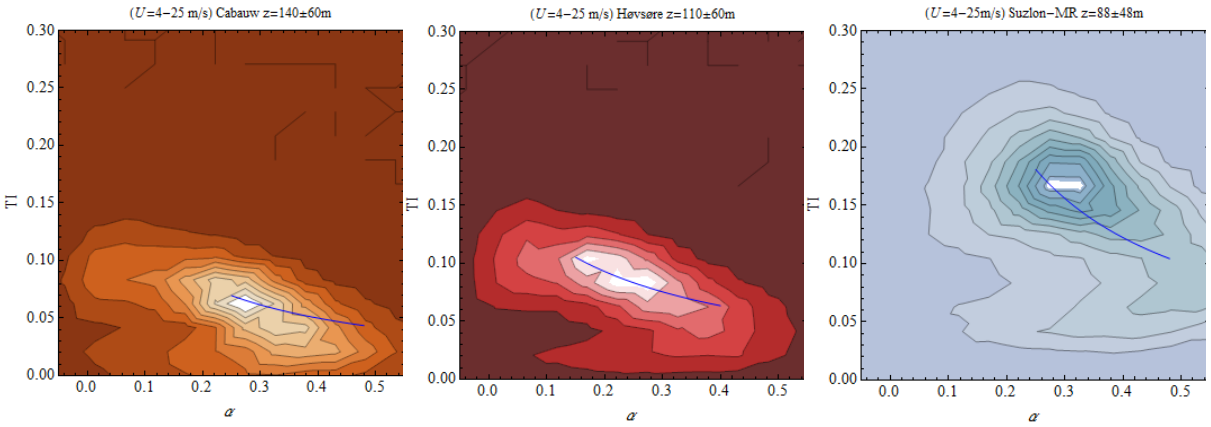

Figure 7. Turbulence intensity and shear exponent distribution, with engineering model (7) overlaid as a blue line. Left (a): Cabauw; center (b): Høvsøre; right (c): site 'MR'.

We can see from figure 7 that the reduced formulation (8) does a fair job reproducing the mean (and most likely) behavior of $\{\alpha, I_U\}$. If we had used (6) for α instead of its definition including Monin-Obukhov functions, we arrive at a form similar to (8), $I_U = I_{U0}(1-\alpha)/(1+\beta\alpha_0)$; however, this form does not give reasonable results, due to not having been practically adjusted to apply above the ASL.

Since we also have an expression for the width of $P(\alpha)$, one can also invert (8) to obtain a model for α in terms of turbulence intensity and wind speed, which is the parameterization employed by [15]. The expression for mean shear exponent following (8) has a form $\alpha = \alpha_0 + (I_{U0}/I_U - 1)/c_\alpha$; this is in contrast with that of [19], who made a fully empirical relation that multiplies α_0 by a stability-based factor.

Despite the turbulence intensity being the dominant driving parameter for most loads calculations, we re-iterate the findings of [15] who used (8) and (3) for a large number of loads simulations: the shear exponent distribution becomes significant for fatigue loads in low-I_U conditions, and also for blade-tip deflection in extreme I_U cases.

3. Loads and output: effect of input distributions

Here we give an example of the effect of varying α upon loads, based on the observed shear exponent-wind speed distribution $P(\alpha,U)$. The analysis is done for the 'tall' Østerild case (80-200m) from lidar, so no turbulence data were observed. In particular the fatigue loads were calculated for the NREL 5MW reference turbine [20] using HAWC-2, for IEC 61400-1 design load cases including normal operation, normal startup/shutdown and failure; this assumed turbulence class A, with 2m/s increments for U and increments of 0.1 for α, with six seeds used for every $\{\alpha,U\}$ pair. The fatigue loads were summed up with weighting according to observed $P(\alpha,U)$.

A sample of flapwise blade-root 1 Hz equivalent moments is given in figure 8, for the wind speed bin from 14–16m/s. For the NREL controller, the load per α is shown in the left-hand plot, indicating e.g. an equivalent moment of ~9200 kN/kNm for α=0.2. In the right-hand plot, the load probability distribution (grey shaded) and the cumulative distribution (black line) is shown for this wind speed bin. One can see that width of $P(\alpha|U)$ for this wind speed range leads to a skewed flapwise load distribution, with the 50% percentile of fatigue load occurring at a value (8900 kN/kNm) several percent lower than that which would be predicted using the standard α of 0.2.

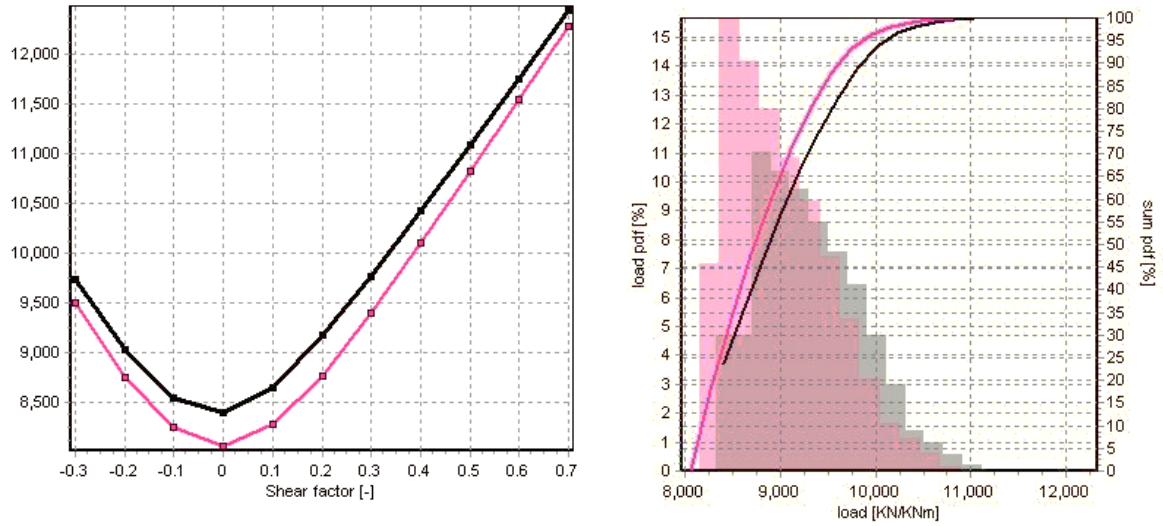

Figure 8. Loads example using observed $P(\alpha,I_U)$, Østerild 'tall' case with NREL controller (black/grey). Left: flapwise load (in KN/KNm) versus α. Right: CDF (line) and PDF (shaded) of load distribution.

Systematic differences of several percent are seen in the damage equivalent fatigue loads (akin to the 14-16m/s result shown in figure 8) for most wind speeds, and the annual energy production (not shown) is more than 10% lower than if one used the standard Weibull distribution with α=0.2. Again, as found in [15], the variability in shear can also have a more pronounced effect in both low and extreme turbulence regimes.

4. Summary and conclusions

Here we have introduced the shear exponent α and connected it with stability and turbulence intensity, also showing its connection with conventional surface roughness. We examine its utility above the atmospheric surface layer, where similarity theory begins to fail, using data from a number of 'tall' sites. The joint statistical behavior of α, wind speed, and turbulence intensity is explored and interpreted, both via the observations and with connection to accepted micrometeorological (i.e. surface-layer and similarity) theory. We find a relationship between typically-averaged (i.e. 10-minute) wind speed and standard deviation of shear exponent, which is useful for modelling the shear for e.g. input to fatigue loads calculations. We also derive the relationship between shear exponent, atmospheric stability, turbulence intensity, and turbulent transport based on the mean turbulent kinetic energy balance, in a way consistent with Monin-Obukhov theory in the constant-flux (ASL) limit. A practical reduction of this relationship is made for application above the ASL, and this leads to a characterization of turbulence intensity in terms of shear exponent (or vice-versa) in a form amenable to use in the IEC 61400-1 standard.

A simple example is also shown which demonstrates the distribution of damage equivalent fatigue loads which arise from the joint distribution of shear exponent and wind speed at one observation site.

Ongoing and future work includes: characterization of veer, its joint distribution with shear exponent, and effect on the loads, as well as a simplified re-formulation of the variability of shear, TI, and veer for application in standards to extreme and fatigue loads estimates.

Acknowledgments

The authors wish to thank Peter Bjørn Andersen for HAWC-2 calculations. We also extend appreciation to Wiebke Langreder and Suzlon for the data from the site 'MR,' and KNMI for use of

the Cabauw mast data. The authors also gratefully acknowledge support from the Danish Energy Technology/Development/Demonstration (EUDP) project 64011-0352, "Demonstration of a basis for tall wind turbine design."

Appendix

A generic two-sided form for stability distributions was found by [10] in terms of the inverse Obukhov length, to be

$$P(L^{-1}) = n_{\pm} C_{\pm} \exp\left[-(C_{\pm} \mid L^{-1} \mid /\sigma_{\pm})^{2/3}\right] \Big/ \left(\sigma_{\pm} \Gamma(\tfrac{5}{2})\right) \tag{A.1}$$

where $\sigma_{\pm} \equiv (g/T_0)\left\langle (\overline{w\theta} - \left\langle \overline{w\theta} \right\rangle_{\pm})^2 \right\rangle^{1/2} \Big/ \left\langle u_{*0} \right\rangle_{\pm}^3$ is the L^{-1} scale (variability), $C_{\pm}$ are constants, and $n_{\pm}$ are the fraction of conditions which are stable ($L^{-1} > 0$) or unstable; "+/-" subscripts indicate values for either stable or unstable conditions.

A probability distribution may be transformed from one variable to another, in this case between α and L^{-1}, via $P(\alpha) = P(L^{-1}) \Big/ \left| d\alpha / dL^{-1} \right|$. Focusing on the higher-shear case of stable conditions (denoted by subscript '+'), from Monin-Obukhov theory (1) can be written $\alpha = \left[\phi(z/L) \Big/ \left(\ln(z/z_0) - \psi(z/L)\right)\right]$, or $\alpha_+ = \left[1 - 5z/L \Big/ \left(\ln(z/z_0) + 5z/L\right)\right]$ under stable conditions. Since

$$\frac{\mathrm{d}\alpha}{\mathrm{d}L^{-1}} = \frac{\alpha}{\phi}\left[\frac{\mathrm{d}\phi}{\mathrm{d}L^{-1}} + \alpha \frac{\mathrm{d}\psi}{\mathrm{d}L^{-1}}\right] \tag{A.2}$$

then

$$P(\alpha) = \pm P(L^{-1}) \frac{\phi}{\alpha} \left| \frac{\mathrm{d}\phi}{\mathrm{d}L^{-1}} + \frac{\phi \, \mathrm{d}\psi / \mathrm{d}L^{-1}}{\ln(z/z_0) - \psi} \right|^{-1} \tag{A.3}$$

where the +/- is for α either increasing or decreasing with L^{-1}. For stable conditions then

$$P_+(\alpha_+) = \pm P_+(L_+^{-1}) \frac{1 + 5zL_+^{-1}}{\alpha_+ 5z \mid 1 - \alpha_+ \mid} \; ; \tag{A.4}$$

inverting the $\{\alpha_+, L_+^{-1}\}$ relation we then find $L_+^{-1} = \left[\alpha_+ \ln(z/z_0) - 1\right] \Big/ \left[5z(1-\alpha_+)\right]$. Subsequently since L_+^{-1} is positive and $\alpha\left(L_+^{-1}\right) < 1$, then $\alpha_0 < \alpha_+ < 1$ where again $\alpha_0 = 1/\ln(z/z_0)$. Finally we have

$$P_+(\alpha_+) = \frac{P_+\left(L_+^{-1}(\alpha_+)\right)}{5\alpha_+ z \mid 1 - \alpha_+ \mid} \left[1 + \frac{\alpha_+ \ln(z/z_0)}{1 - \alpha_+}\right] \tag{A.5}$$

with $P(L_+^{-1})$ given by (A.1), where the arguments and subscripts all correspond to the stable (+) side distribution.

References

[1] International Electrotechnical Commission 2005 *IEC 61400-1 Ed.3: Wind Turbines – Part 1: Design Requirements* (Geneva: IEC Central Office)

[2] Beljaars A C M and Bosveld F C 1997 Cabauw data for the validation of land surface parameterization schemes *J. Clim.* **10** 1172–1193

[3] Jørgensen H E, Mikkelsen T, Gryning S-E, Larsen S, Astrup P and Sørensen P E 2008 'Measurements from Høvsøre met mast'. *Technical Report Risø-R-1592(EN)* (Roskilde, DK: Risø National Laboratory)

[4] Gómez Arranz P and Vesth A 2013 *Site Calibration report, Østerild. DTU Wind Energy I-1048* (DTU Wind Energy WTT I; No. 1048(EN)) 116 pp.

[5] Simpson IJ, Thurtell GW, Neumann HH, Den Hartog G and Edwards GC 1998 The validity of similarity theory in the roughness sublayer above forests. *Boundary-Layer Meteorol*. **87** 69–99
[6] Dellwik E, Mann J and Bingöl F 2014 Flow distortion at a dense forest edge *Q.J.R. Meteorol. Soc.* **140** (679B) 676–686
[7] Irwin J S 1979 A theoretical variation of the wind profile power-law exponent as a function of surface roughness and stability. *Atmos. Environ.* **13** 191–194
[8] Petersen E L, Mortensen N G, Landberg L, Høstrup J and Frank H P 1998 Wind power meteorology. Part II: siting and models *Wind Energy* **1** 55–72
[9] Wharton S and Lundquist J 2012 Assessing atmospheric stability and its impacts on rotor-disk wind characteristics at an onshore wind farm *Wind Energy* **15** 525–546
[10] Kelly M and Gryning S-E 2010 Long-term mean wind profiles based on similarity theory *Bound.-Layer Meteorol.* **136**(3) 377–390
[11] Hasager C B and Jensen N O 1999 Surface-flux aggregation in heterogeneous terrain *Q.J.R. Meteorol. Soc.* **125** 2075–2102
[12] Beljaars A C M, Brown A R and Wood N 2004 A new parametrization of turbulent orographic form drag *Q.J.R. Meteorol. Soc.* **130** 1327–1347
[13] Mahrt L 1996 The bulk aerodynamic formulation over heterogeneous surfaces *Bound.-Layer Meteorol.* **78** 87–119
[14] Pardyjak E, Mahrt L, Jensen N O, Fernando H, Sun J, Jørgensen H E and Vickers D 2001 Determination of the surface drag coefficient *Bound.-Layer Meteorol.* **99**(2) 249–276
[15] Dimitrov N K, Natarajan A and Kelly M 2014 Model of wind shear conditional on turbulence and its impact on wind turbine loads *Wind Energy* (**in press**)
[16] Foken T 2004 "50 years of the Monin-Obukhov similarity theory" *16th Symposium on Boundary Layers and Turbulence* (Portland, ME, US: Amer.Met.Soc.)
[17] Kaimal J C and Finnigan J J 1994 *Atmospheric boundary layer flows: their structure and measurement* (New York: Oxford University Press) 289 pp.
[18] Zilitinkevich S and Esau I 2005 Resistance and heat-transfer laws for stable and neutral planetary boundary layers: old theory advanced and re-evaluated *Q.J.R. Meteorol. Soc.* **131** 1863–1892
[19] Newman J F and Klein P M 2014 The Impacts of Atmospheric Stability on the Accuracy of Wind Speed Extrapolation Methods *Resources* **3** 81–105
[20] Jonkman J, Butterfield S, Musial W, and Scott G 2009 *Definition of a 5-MW reference wind turbine for offshore system development* (National Renewable Energy Lab tech.report NREL/TP-500-38060).
[21] Lenschow D H, Mann J and Kristensen L 1994 How long is long enough when measuring fluxes and other turbulence statistics? *J.Atmos.Ocean Tech.* **11** 661–673
[22] Sathe A, Mann J, Barlas T, Bierboms W A A M, and van Bussel G J W 2013 Influence of atmospheric stability on wind turbine loads *Wind Energy* **16** 1013–1032